

Chaos control in multistable delay-differential equations and their singular limit maps

Boualem Mensour* and André Longtin†

Département de Physique, Université d'Ottawa, 150 Louis Pasteur, Ottawa, Ontario, Canada K1N 6N5

(Received 17 July 1997; revised manuscript received 31 March 1998)

The multistability exhibited by first-order delay-differential equations (DDE's) at large delay-to-response ratios R is useful for the design of dynamical memory devices. This paper first characterizes multistability in the Mackey-Glass DDE at large R . The extended control of its unstable periodic orbits (UPO's), based on additional feedback terms evaluated at many times in the past, is then presented. The method enhances the control of UPO's and of their harmonics. Further, the discrete-time map obtained in the singular perturbation limit of the controlled DDE is useful to characterize the range of parameters where this extended control occurs. Our paper then shows how this singular limit map leads to an improved method of controlling UPO's in continuous-time difference equations and in discrete-time maps. The performance of the method in the general contexts of extended additive and parametric control is evaluated using the logistic map and the Mackey-Glass map. The applicability of the method is finally illustrated on the Nagumo-Sato discrete-time neural network model. [S1063-651X(98)09707-4]

PACS number(s): 05.45.+b, 02.30.Ks, 42.65.Pc, 42.79.Ta

I. INTRODUCTION

Multistability in a dynamical system is the coexistence of multiple attractors. This property implies that qualitatively different asymptotic solutions can result from changes in the initial conditions. Multistability in delay-differential systems has received recent attention because it enables such systems to act as memory devices, an idea first suggested by Ikeda and Matsumoto [1]. For the simple first-order delay-differential equations of interest in many applications [2,3], multistability appears when the delay τ is much greater than the response time τ_r of the system. Different periodic solutions, chaotic solutions, or both may then coexist for a given set of equation parameters [2,4].

Interest in multistability in delay-differential equations (DDE's) arises in the context of nonlinear control, such as occurs in physiological systems [3,5,6] and optical or neural network systems with delayed feedback [7]. For example, prescribed periodic solutions can be stored as oscillatory patterns in the electromagnetic field of a laser cavity [8,9] or in the firing activity in models of neural recurrent feedback loops [10] by choosing appropriate initial conditions. Such multistability has further been demonstrated in electronic circuits [11,12]. Unstable periodic solutions (UPO's) can also be used to store prescribed patterns if they are first stabilized by chaos-control techniques [13] such as those based on additive delayed feedback [14]. The chaotic regime makes the memory storage very versatile, due (1) to the existence of an infinite number of UPO's, some of which coexist with one or more chaotic attractors, and (2) to the adjustability of the period of UPO's through variations of the intrinsic delay (as distinguished from the second delay for chaos control [14]). Such feedback has further been shown to allow the stabiliza-

tion of UPO's in delay-differential models of cortical function [5].

The first part of our paper (Secs. II and III) discusses chaos control in the Mackey-Glass DDE [3] using a second delayed feedback loop [14], as well as its generalization in terms of "extended control," where feedback from values of the state variable at several regularly spaced times in the past is used [15]. The number of harmonics of the fundamental wave form which coexist in the Mackey-Glass DDE is also studied in order to identify the subset of the infinite number of UPO's which can realistically be (1) controlled using delayed-feedback chaos control, and (2) used for information storage purposes.

The second part of our paper (Secs. IV and V) presents a chaos-control method for discrete-time maps. It is based on the dynamics of the DDE in the singular limit where the delay-to-response time ratio $R \rightarrow \infty$. We discuss its performance, and illustrate it on the logistic map as well as on the "Mackey-Glass" map which results from the singular limit of the Mackey-Glass DDE. We also illustrate the method on a discrete-time neural network model known as the Nagumo-Sato model [16] (see also Ref. [17]). We then improve our method using extended control [15]. With this improvement, orbits of even higher periodicity (i.e., of higher bifurcation order in a period-doubling sequence) can be stabilized. Our method is found to allow the control of UPO's in these maps over larger parameter ranges than those found with other existing methods [14,15,18].

We further bridge results in the two parts of our paper by showing that, under certain conditions, chaos control in the DDE can be understood using the finite-dimensional discrete-time map suggested by our control method. Singular limit maps have been shown to be useful in understanding certain aspects of the behavior of the associated DDE's (see, e.g., Refs. [4,19,20]). This map predicts the range of parameters for which control occurs; the accuracy of this prediction increases with R . This result has previously been discussed for simple delayed feedback control [14] in Ref. [13], and is shown here in the context of extended delayed control [15].

*Present address: Centre de Recherche de l'Hôpital du Sacré-Coeur de Montréal, 5400 boul. Gouin Ouest, Montréal, Québec, Canada H4J 1C5.

†Author to whom correspondence should be addressed.

One of our goals in developing this control method is to understand multistability and UPO control in models of spatially distributed excitable cell assemblies, such as those found in nervous and cardiac tissue (see, e.g., Ref. [21] for a recent review). The possibility of controlling, using nonlinear dynamical techniques, disorders such as epilepsy or heart arrhythmias, when the underlying systems indeed exhibit, e.g., chaotic dynamics in health or in disease, is exciting [22]. Models of such cell assemblies often rely on a simplified discrete-time map description of the single cell dynamics (compared to, e.g., complex Hodgkin-Huxley dynamics) to make them computationally efficient and/or analytically tractable. These have been used as the fundamental computational elements of artificial neural networks as in, e.g., Refs. [16,17,23]. Further, our results for DDE's and their limiting maps will help understand UPO controllability in physiological, optical, and other systems, involving one or many delayed feedback loops [24–26].

This paper is organized as follows. Section II discusses multistability and hysteresis in the Mackey-Glass (MG) DDE at large delay. It illustrates the kinds of solutions that can be obtained in such equations; these same kinds of solutions occur through chaos control techniques such as that described in Sec. III. This section also reviews the “extended control” method of Ref. [15], and shows how it enables the control of finely structured UPO's of the Mackey-Glass DDE, such as those corresponding to higher bifurcation orders. In Sec. IV we present our improved method of controlling discrete-time maps, inspired from the control of the DDE in the singular perturbation limit. The range of control in parameter space is studied analytically for fixed point control in both the additive and parametric “extended control” cases. We also discuss how the controlled map ($R \rightarrow \infty$) reveals information on how to control the DDE (finite R). In Sec. V, we apply our improved control method to a chaotic discrete-time neural network based on the Nagumo-Sato model. The paper concludes in Sec. VI.

II. MULTISTABILITY IN THE MACKEY-GLASS DDE

A. Dynamical equations and numerical methods

We focus on first-order delay-differential equations of the form [2,3]:

$$\dot{x}(t) = -bx(t) + F(x(t-\tau)), \quad (1)$$

where τ is the intrinsic delay in the feedback loop and $\tau_r = 1/b$ is the response time. We define the delay-to-response-time ratio $R = \tau/\tau_r = b\tau$. This equation describes an infinite-dimensional dynamical system, and can be solved by specifying an infinite number of initial conditions (i.e., a function) over the delay interval.

We have used a fixed step fourth-order Runge-Kutta algorithm for all numerical integrations of this system. The time step must be small enough to integrate the solutions properly over the fastest time scale b^{-1} . In particular, for periodic solutions such as controlled UPO's, square-wave-like solutions are often encountered, in which constant “plateaus” are connected by rapid transitions of duration $O(b^{-1})$; these transitions can be seen as “boundary layers” in which the derivative is of order $O(R^{-1})$. For $b=0.1$, as

below, accurate solutions on every time scale can be obtained for any delay by using a 0.1-s integration time step.

One can obtain a good idea of the solutions and of their controllability for large R by using instead a larger time step. By “controllability” we mean a measure of the range of parameters (such as a hypervolume in parameter space) over which control occurs to within a specified error magnitude. The use of a larger time step will not produce accurate transitions between plateaus, but the plateau values will be accurate. As R increases, the duration of these rapid transitions becomes negligible compared to the duration of plateaus themselves in periodic orbits or controlled UPO's. Alternately, one can rescale time with $\tau \rightarrow \tau'/\epsilon$, $t \rightarrow t'/\epsilon$, yielding

$$b^{-1}\epsilon \frac{dy(t')}{dt'} = -y(t') + b^{-1}F(y(t'-\tau')), \quad (2)$$

where $x(t) \equiv y(t')$. With this transformation, the DDE can be studied numerically at large delay (for example, $\tau=300$, with $b^{-1}=10$) in terms of an equivalent DDE at smaller delay (e.g., if $\epsilon=0.1$, $\tau'=30$, with an equivalent time scale $\epsilon b^{-1}=1.0$), with a time step ϵ^{-1} times smaller for fully accurate solutions, or larger for an approximate solution as discussed above (the ratios $R=b\tau$ and $R'=b\epsilon^{-1}\tau'$ remain the same).

Most studies of multistability in DDE's have focused on the Ikeda equation [1,2,4]. In the present study, multistability in the Mackey-Glass DDE (MG-DDE) is of interest, with particular emphasis on its UPO's, since we wish to control these unstable wave forms for large delays. We thus first have to verify whether the basic multistability properties in the MG-DDE are similar to those of the Ikeda equation. Our results indicate that this is so, and are summarized below. This is expected, as comparisons of previous studies [4,9,13] indicate that the two systems are similar with respect to the organization of the UPO's and with respect to the control of low period UPO's.

The Mackey-Glass equation is [3]

$$\begin{aligned} \dot{x}(t) &= -bx(t) + F(x(t-\tau)) \\ &= -bx(t) + ax(t-\tau)/(1+x^c(t-\tau)), \end{aligned} \quad (3)$$

with $c=10$ and $b=0.1$ (constant throughout our paper) at large delay $\tau=300$ (for example). It is typically difficult to find different initial conditions that lead to the different coexisting solutions for a given set of parameters. It is easier to obtain an idea of the shape of solutions that may coexist by keeping the initial condition fixed and then varying the feedback parameter a slightly (Fig. 1; see also Ref. [4]); the resulting solutions are not coexistent, but are representative of coexisting solutions which could be found for fixed parameters by trying different initial functions.

A Hopf bifurcation occurs at $a=0.125$. For a slightly larger than this value, the oscillation has already grown into a square-wave-like wave form, which we refer to as the “fundamental solution,” with period $T_1 \approx 2\tau$. As a increases further, this solution undergoes a period-doubling sequence, where the two plateaus of the square wave are replaced by four plateaus, then eight, etc. At the same time as this fundamental solution goes through its period-doubling sequence, other solutions come into existence [27], which

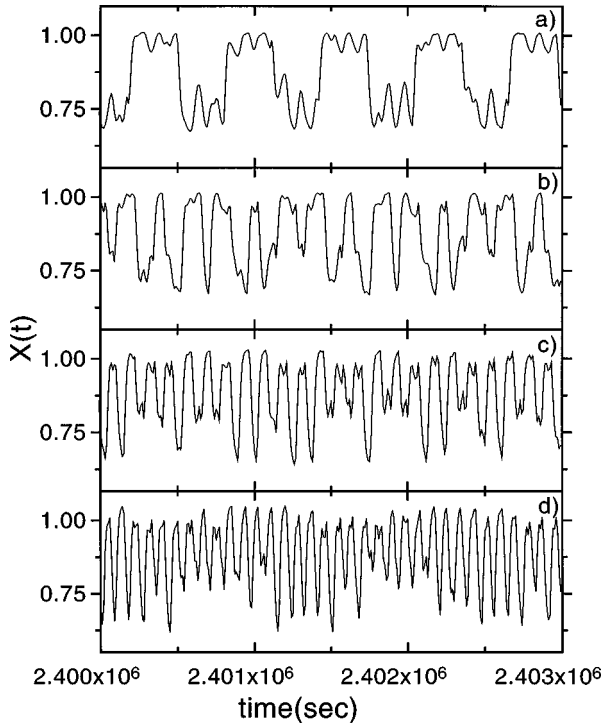


FIG. 1. The different solutions of Eq. (3) corresponding to the different harmonics for $\tau=300$. The same constant initial function $x_0=0.95$ on $(-\tau,0)$ was used in each case. (a) Fundamental solution ($a=0.14$). (b) Third harmonic ($a=0.141$). (c) Fifth harmonic ($a=0.143$). (d) Seventh harmonic ($a=0.1467$).

independently undergo period-doubling cascades. They are usually not visible unless special initial conditions that approximate the shape of the solution are chosen. The third harmonic of the fundamental, with period $T_1/3$, appears at $a=0.1317$. The fifth harmonic appears at $a=0.1376$, and finally the seventh at $a=0.1425$.

When a reaches the period-doubling accumulation point of the fundamental at $a_\infty \approx 0.138$, the square-wave solution becomes chaotic. However, it still has a basic square-wave like shape, as seen in Fig. 1(a). If a is further increased, this square-wave solution becomes unstable, and successive chaotic ‘‘harmonics’’ with basic ‘‘period’’ (they are not exactly periodic) close to T_1/n can be observed (n is an odd integer representing the harmonic order). The solution jumps first to the third harmonic at $a=0.141$, then to the fifth at $a=0.1414$, then to the seventh at $a=0.1466$, and finally to developed chaos at $a=0.1485$.

Figure 1 illustrates the different chaotic harmonics $f_0 = T_1^{-1}$, $3f_0$, $5f_0$, and $7f_0$. Note that the initial function in all cases was chosen here to be the same constant; thus this figure does not indicate multistability; it merely shows typical solutions over a certain range of a which exist and become unstable as a increases, and which chaos control should be able to stabilize. Other (but not all) initial functions will also yield four similar solutions for the same four values of a .

B. Multistability and hysteresis

Figure 2 demonstrates multistability by showing the coexistence of several harmonic solutions for the same value of

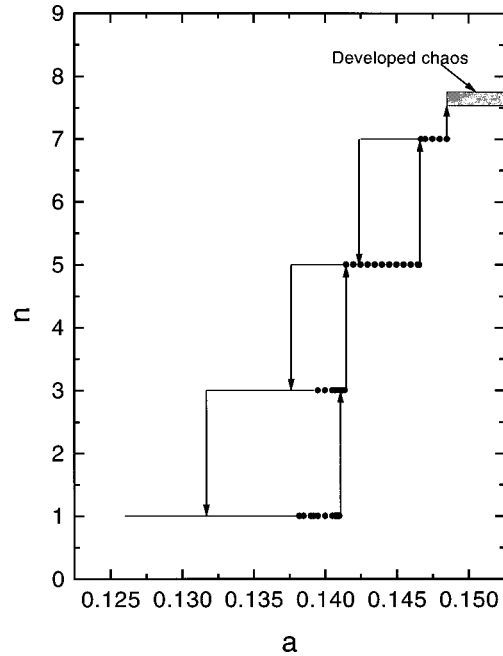


FIG. 2. Domains of coexistence and hysteresis of harmonics in Eq. (3) for $\tau=300$. The solid and dotted lines indicate the periodic and chaotic solutions, respectively. The initial conditions are chosen from the plateaus of the square wave solutions of period-2 and -4 orbits. Since seemingly stable solutions converge to simpler harmonics after a long time, transients of 7000 delays have been discarded to identify stable solutions.

a . The range of a over which the n th harmonic is stable can be found numerically by splitting the initial delay function into n equal subintervals, with the function taking on constant values (‘‘plateaus’’) within each subinterval. The values of these plateaus in this piecewise-constant initial function are generally chosen from those in the fundamental square-wave-like periodic solution. The resulting asymptotic solution is observed for a given value of a ; this parameter is then changed slightly, and the process is repeated until one can no longer find that particular harmonic.

Our results indicate that solution coexistence can be (1) between chaotic orbits and periodic orbits, such as between the chaotic fundamental, the chaotic third harmonic, and the periodic fifth harmonic when $a=0.141$; or (2) between periodic orbits, e.g., when $a=0.1376$ (see Fig. 3). This is also true for the Ikeda model [4]. In fact, the organization of the multistable orbits, and of the hysteresis loops between them, is very similar to that seen in the Ikeda equation [4]. These loops follow from the transitions between harmonics as a increases and decreases. Not all harmonics coexist at the same value of a . For example, the seventh harmonic solution coexists only with the fifth harmonic, while the latter coexists with the third harmonic and the fundamental (see Fig. 2).

The number of coexisting harmonic solutions has been shown to increase linearly with the delay in the Ikeda equation, where it is in fact proportional to the ratio of $\tau/\tau_r = b\tau$ [4]. We expect that the MG-DDE will also have this property, in view of the strong similarity between the two systems [4,9,13] (we note that another recent study [28] supports this similarity from the point of view of the spectral properties of the solutions of both systems with increasing

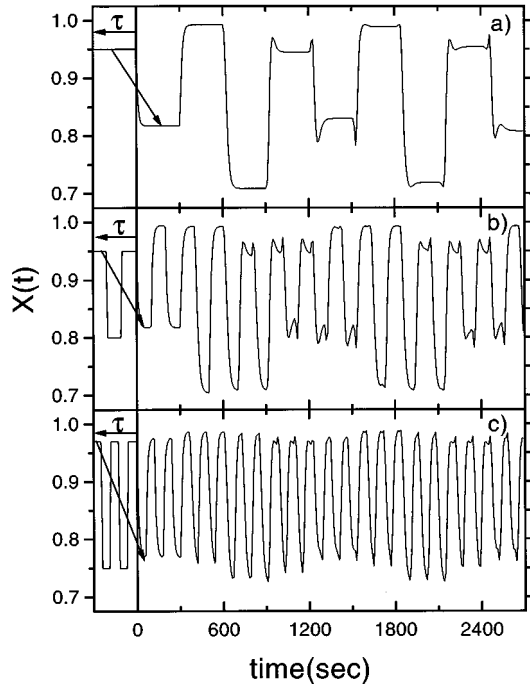


FIG. 3. Multistability in Eq. (3). Three periodic solutions coexist for $a=0.1376$ and $\tau=300$: (a) the fundamental, (b) the third harmonic, and (c) the fifth harmonic. These solutions are obtained with three different piecewise constant initial functions and all other parameters fixed. The delay τ is subdivided respectively into one, three, and five small plateaus of equal width.

delay). While our simulations (not shown) indicate that the number of coexisting harmonics does increase with the delay in the MG-DDE, more simulations are needed to ascertain whether the relationship between this number and the delay is linear as for the Ikeda equation.

For the present study, and those of information storage as well, we rather concentrate on the facts that multistability exists, and that it is limited, i.e., a finite number of solutions coexist. For a given delay (or ratio R since b is constant in our study), there is a finite number of harmonics, periodic or chaotic, that can coexist. This number is three for $\tau=300$, according to Fig. 2. Also, for this delay (and other parameters fixed, except for a), the highest harmonic that we have observed is $7f_0$. Increasing a further produces chaotic solutions in which it is difficult to discern any particular harmonic structure.

Thus, for $\tau=300$, there is a maximum number of harmonics $n_{\max}=4$ that can be encountered as a is varied, corresponding to f_0 , $3f_0$, $5f_0$, and $7f_0$. The maximum number of plateaus in the initial condition which can evolve independently of one another is seven, the harmonic of highest frequency which can be observed. Thus, for these parameters, seven is the maximum number of plateaus in the initial condition that are available for storing initial values to produce a prescribed pattern. Solutions with more than seven plateaus will merge to one of the stable solutions in Fig. 2. Thus, there is a limit to the number of harmonic solutions that can be observed for a given value of a , i.e., to the number of plateaus n in the initial function that can evolve in time without merging. Knowledge of this limit is important for memory storage applications such as those in Refs. [9,13];

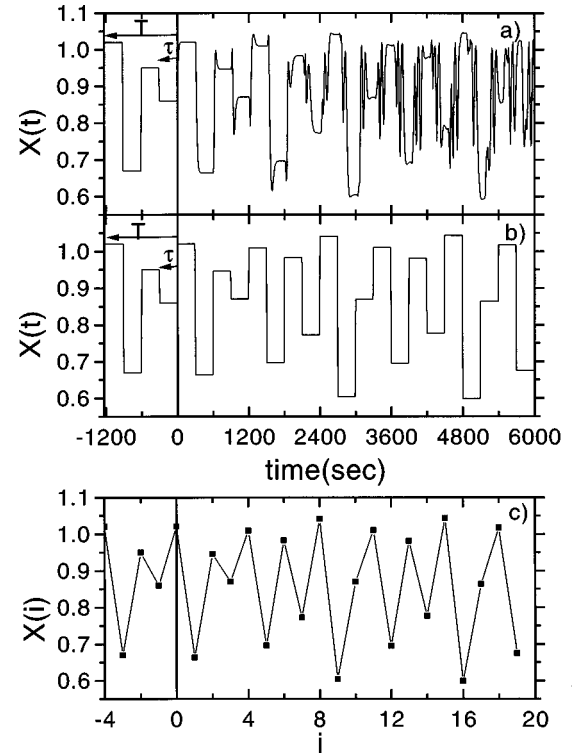


FIG. 4. Numerical solutions of Eq. (3) for $a=0.145$ without control ($K=0$, $r=0$) using piecewise constant initial conditions. (a) Chaotic solution of the DDE [Eq. (9)] for $\tau=300$. (b) Chaotic solution of the CTDE [Eq. (12)] for $\tau=300$. (c) Chaotic solution of the map [Eq. (14)]. Note that the solutions in (b) and (c) look periodic because the initial function makes them initially follow an UPO.

these latter studies have shown that this limit increases with R .

Interestingly, we have found that the ratio R/n_{\max} is approximately the same in both the MG and Ikeda DDE's in the parameter ranges studied. In the MG-DDE with $\tau=300$ and $\tau_r=10$ (i.e., $R=30$), this ratio is 4.28, while in the Ikeda DDE [4] with $\tau=40$ and $\tau_r=1$ (i.e., $R=40$), this ratio is 4.44 (our simulations of the Ikeda equation show five harmonics, i.e., $n_{\max}=9$, while the number of harmonics found in [4] was four). It is thus likely that the proportionality between n_{\max} and R is similar in both systems; further work is necessary to see if the proportionality constant is the same or is dependent on the particular feedback used. In Sec. III, we study the control of the UPO's that arise as the multistable solutions studied in this section become unstable following parameter changes (typically increases in a).

III. CONTROLLING MULTISTABLE SOLUTIONS IN THE MACKEY-GLASS DDE

A. A second delayed feedback control

Equation (3) has one delayed feedback control term. Its solutions at large R are chaotic over a wide range of parameters [see Fig. 4(a)]. As $\tau \rightarrow \infty$ (the limit of interest in our study), or $\epsilon \rightarrow 0$ in Eq. (2), $R \rightarrow \infty$ and the dynamics are governed by the resulting continuous-time difference equation (CTDE)

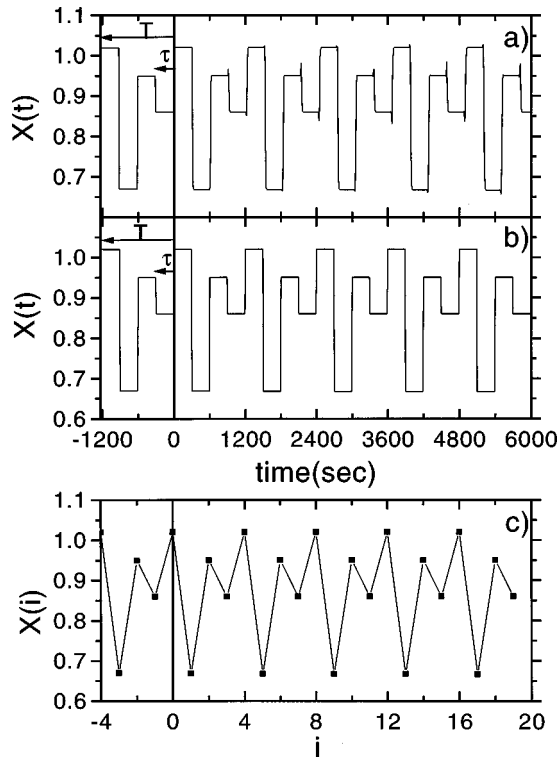


FIG. 5. Control of the Mackey-Glass DDE [Eq. (3)] and of its corresponding CTDE and map for $a=0.145$, $K=0.2$, and $r=0.8$; piecewise constant initial conditions are used. (a) Controlled P_4 orbit of Eq. (9) for $\tau=300$ and $T=1225.6$. (b) Controlled P_4 orbit for the CTDE ($b\tau \rightarrow \infty$) [Eq. (12)] for $\tau=300$ and $T=1200$. (c) Controlled P_4 orbit for the map [Eq. (14)].

$$x(t) = b^{-1}F(x(t-\tau)). \quad (4)$$

In this formulation, any point in a given delay interval evolves in time from one delay interval to the next, independently of its neighboring points in that delay interval. The solution can thus be discontinuous. For constant initial conditions, the solutions are composed of plateaus. The evolution of a given point from one delay interval to the next is given by the map obtained by discretizing time in units of τ in Eq. (4):

$$x(i) = b^{-1}F(x(i-1)). \quad (5)$$

The dynamics of Eqs. (4) and (5) are also chaotic [see Figs. 4(b) and 4(c)]. If a second delayed control [14], or better still, an “extended control” [15,29,30] (see below) is properly applied, the chaotic harmonics as well as UPO’s of the DDE, CTDE, and map can be made periodic. This is shown in Fig. 5 for a period-4 “ P_4 ” orbit, for which the map cycles between four values, the CTDE between four plateaus, and the DDE between four plateaus connected by abrupt yet smooth transitions. In the following, N designates the number of points in the orbit of the singular limit map, or, alternately, the number of values through which the plateaus in the DDE or CTDE cycle. We will thus refer to a “ P_N ”-type solution.

Control is achieved here by adding a second feedback $D(t) \equiv K[x(t-T) - x(t)]$ in Eq. (1) [14], where $T > \tau$ is the

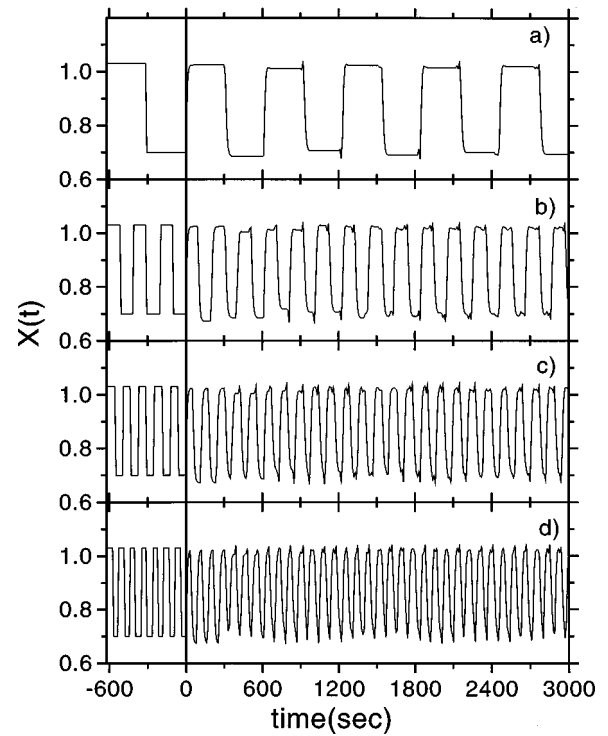


FIG. 6. Control of the multistable solutions in Fig. 1 for $a=0.15$, $K=0.05$, and $r=0$. The period T in each case is chosen slightly different from the period of the UPO P_2 ($T=615.9$), since the ratio $T/(2n\Delta t)$, which is the number of points on each plateau in the initial condition on $-T < t < 0$, should be an integer to allow the integration (n is the harmonic order). This procedure does not affect the basic result. (a) The controlled P_2 orbit ($T=615.8$). (b) The controlled third harmonic ($T=615.6$). (c) The controlled fifth harmonic ($T=616.0$). (d) The controlled seventh harmonic ($T=614.6$).

period of the unstable (periodic or chaotic) fundamental solution, and K is the control parameter. The dynamics then become

$$\dot{x}(t) = -bx(t) + F(x(t-\tau)) + K[x(t-T) - x(t)]. \quad (6)$$

One has the choice of controlling a variety of UPO’s; the ones of interest in our work are the fixed point, the fundamental square-wave periodic solution, harmonics of this solution, period-doubled versions of the fundamental solution, and the harmonics of these period-doubled solutions. All these solutions further form a continuum as the period of the fundamental solution varies, as determined by the hysteresis diagram Fig. 2 (this period is proportional to τ [9,13]).

To control a harmonic of order n of the fundamental solution, the initial function in the interval $-T < t < 0$ is split into $2n$ equal plateaus. The values of x attributed to these plateaus are chosen from the unstable fundamental solution. Figure 6 shows the coexistence of the controlled fundamental UPO of period $T=615.9$, and its harmonics when $a=0.15$. Such solutions are important for memory storage purposes, since a finite “message” can be stored into a stable periodic solution [9,10] or a stabilized UPO [13].

One can also select to stabilize the UPO P_N of period T , and use a harmonic solution of order n with $1 < n < n_{\max}$ as the initial function over one delay interval τ . It is further

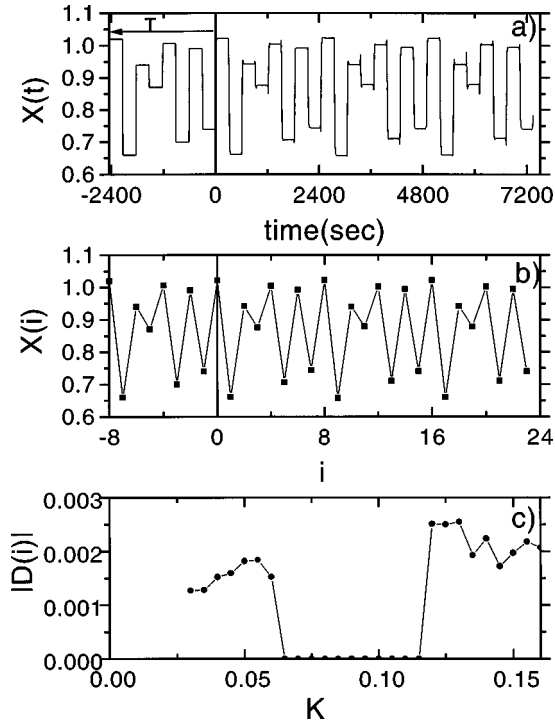


FIG. 7. (a) Extended control of the P_8 orbit of the MG DDE Eq. (9) for $a=0.145$, $K=0.08$, and $r=0.9$, with $\tau=300$ and $T=2447.2$. The initial condition on $-T < t < 0$ is a piecewise constant function corresponding to the wave form of P_8 , as predicted by the map Eq. (14) in (b). (b) Extended control of the P_8 orbit of the map with Eq. (14) using $L=8$. (c) Prediction of control in the DDE using the dispersion $|D(i)|$ vs K for the P_8 orbit of the map [Eq. (14)]. Transients of 5000 periods have been discarded.

possible to minimize transients in the evolution toward a harmonic solution by specifying the initial function in the whole interval $-T < t < 0$, instead of the usual $-\tau < t < 0$. This is done simply by copying the initial function on $(-\tau, 0)$ to the previous intervals of duration τ right up to time $-T$. We denote by N_{\max} the maximum number of plateau values through which the stabilized UPO can cycle in one period. N_{\max} depends on the bifurcation order of the particular wave form. For example, after three period doublings starting from the fixed point, $N_{\max}=8$. Figure 7 illustrates the control of a P_8 orbit for the DDE, as well as for the associated singular limit map. It also illustrates the behavior of the dispersion $|D(i)|$ for the map (absolute value of the applied perturbation averaged over time) as a function of K . It is seen that this quantity falls to zero for a range of K values. This corresponds to the range of stable control of P_8 .

The maximum number of patterns which can be stored, or ‘‘storage capacity,’’ is $(N_{\max})^{N_{\max}}$, since each ‘‘bin’’ or plateau of a harmonic can take on one of N_{\max} values. This capacity is limited, since periodic orbits corresponding to higher bifurcation orders are difficult to control using only one previous state at time $t=T$. Section III B illustrates the notion of capacity in the context of extended control.

B. Extended control

Improving the control of finer UPO’s in delay-differential equations can, among other uses, increase memory storage

capacity by using the multistability of the controlled orbits. To achieve such improved control, we use the method of extended control, proposed originally for maps [15], and subsequently for ordinary differential equations [29,30]. This method generalizes the feedback term in Eq. (6) to many previous states:

$$D(t) = K \left[(1-r) \sum_{m=1}^{\infty} r^{m-1} x(t-mT) - x(t) \right] \quad (7)$$

where $0 \leq r < 1$ is an adjustable parameter. This can be rewritten as

$$D(t) = K[x(t-T) - x(t)] + rD(t-T). \quad (8)$$

The DDE with extended control is thus governed by

$$\dot{x}(t) = -bx(t) + F(x(t-\tau)) + D(t), \quad (9)$$

$$D(t) = K[x(t-T) - x(t)] + rD(t-T).$$

This system of equations can be solved by specifying the initial function for $x(t)$ and $D(t)$ in the interval $-T < t < 0$. The parameter r can be tuned to yield the largest interval of K values over which an UPO is controllable. To minimize transients, $x(t)$ is given its average asymptotic values on each plateau predicted by the map [see Eq. (14) below], and $D(t)$ is given its asymptotic value 0. Figure 5(a) shows the control of the P_4 orbit in the MG-DDE [Eq. (9)] for $a=0.145$ and $\tau=300$. The control interval for, e.g., $r=0.8$ is $0.07 \leq K \leq 0.53$, which is large compared with $0.04 \leq K \leq 0.11$ for $r=0$. We will see that this range is close to that over which the singular limit map can be controlled (see Fig. 12 for P_4 , and also Fig. 9 in the case of control of the fixed point).

We illustrate the notion of ‘‘storage capacity’’ with an example. For $\tau=300$, n_{\max} is 7 (Figs. 2 and 6). If $r=0$, $N_{\max}=4$, but, if $r=0.9$, $N_{\max}=8$. Thus, using extended control for the $\tau=300$ case ($R=30$), storage capacity is increased by a factor of 128. For $\tau=300$, other UPO’s with $N > 8$ are very difficult to control in the DDE due to the continuity of the solution imposed by the dynamical equations as well as numerical accuracy. In the map and CTDE, however, (see Sec. IV), such solutions can be controlled up to $N=16$ for $a=0.145$. The control of solutions with higher N are then limited by numerical accuracy.

IV. METHOD FOR DISCRETE-TIME CHAOS CONTROL

In this section, we show that the asymptotic solution and the controllability of the DDE for large but finite delay are predicted by the singular limit dynamics ($b\tau \rightarrow \infty$). In turn, these dynamics provide a general method of controlling any discrete-time dynamical system. We should emphasize here that our goals in controlling UPO’s in difference and delay-differential dynamical systems lie more in the context of controlling known systems such as lasers or simple neural networks, and, e.g., exploiting their multistability properties for, e.g., storage applications, rather than of controlling unknown systems. Thus we are assuming throughout that we have *a priori* knowledge of a good model of the system to be controlled. We first present our general discrete-time control

method, then study its analytical properties for additive and parametric control, and finally discuss its usefulness for studying UPO control in the DDE.

A. Method

Using the rescaling property Eq. (2), the controlled DDE [Eq. (9)] can be written as

$$b^{-1}\epsilon\dot{y}(t') = -y(t') + b^{-1}\{F(y(t' - \tau')) + E(t')\}, \quad (10)$$

$$E(t') = K[y(t' - T') - y(t')] + rE(t' - T'),$$

where $\epsilon t = t'$, $\epsilon\tau = \tau'$, $\epsilon T = T'$, $x(t) \equiv y(t')$, and $D(t) \equiv E(t')$. Note that the term $b^{-1}\epsilon\dot{y}(t')$ is all the more negligible the smaller $b^{-1}\epsilon$ is, and thus the larger b is to begin with. Afterwards, and for simplicity, we resubstitute into Eq. (10) the original variables $x(t)$ and $D(t)$ instead of $y(t')$ and $E(t')$. In the singular limit $b\tau \rightarrow \infty$ (i.e., $b^{-1}\epsilon \rightarrow 0$), Eq. (10) becomes equivalent to a controlled CTDE

$$x(t) = b^{-1}\{F(x(t - \tau)) + D(t)\}, \quad (11)$$

$$D(t) = K[x(t - T) - x(t)] + rD(t - T),$$

which can be rewritten as

$$x(t) = (b + K)^{-1}\{F(x(t - \tau)) + Kx(t - T) + rD(t - T)\},$$

$$D(t) = (b + K)^{-1}\{K[bx(t - T) - F(x(t - \tau))] + brD(t - T)\}. \quad (12)$$

For constant initial conditions, the solutions are composed of plateaus. The evolution of each point on a plateau is given by the map obtained by discretizing time in units of τ in Eq. (11):

$$x(i) = b^{-1}\{F(x(i - 1)) + D(i)\}, \quad (13)$$

$$D(i) = K[x(i - L) - x(i)] + rD(i - L),$$

which can again be rewritten as

$$x(i) = (b + K)^{-1}\{F(x(i - 1)) + Kx(i - L) + rD(i - L)\}, \quad (14)$$

$$D(i) = (b + K)^{-1}\{K[bx(i - L) - F(x(i - 1))] + brD(i - L)\},$$

where L is an integer that represents the period of the UPO of the map. The initial condition is specified in the interval $-L < i < 0$. When the control for a selected UPO is achieved, the perturbation $D(i)$ becomes exactly zero in the CTDE case (in contrast to the differential dynamics case where it is small but finite). The behavior of $D(i)$ for this map predicts the controllability of the DDE at large R (Figs. 7(c) and 12 below).

We show below that this method of controlling maps, inspired by the singular limit of the controlled DDE as well as by the work in Refs. [14,15], allows, in comparison with other methods, more complicated orbits to be controlled; it also allows control of a given solution to within a certain error magnitude over a broader range of parameters. It is also

practical since it can access a large range of the control parameter K and intrinsic feedback parameter a , as illustrated in the next sections. The enhanced range of control stems from the timing of the applied perturbation. For example, in the method of Ref. [15], and the previous methods on which it is based (see Secs. IV B and IV C), time in Eq. (7) is discretized, and UPO's in, e.g., the logistic map $x(i) = F(x(i - 1)) = \mu x(i - 1)(1 - x(i - 1))$ are controlled using feedback perturbations of the parameter $(\mu + d(i - 1))$, where

$$d(i - 1) = K[x(i - 1) - x(i - 1 - L)] + rd(i - 1 - L). \quad (15)$$

This perturbation depends on the previous times $(i - 1)$ and $(i - 1 - L)$; in our method, the perturbation depends on the more recent times (i) and $(i - L)$ [Eqs. (13) and (14)], which allows better control.

A priori, one might expect that causality is violated in our method, since a perturbation involving $x(i)$ is used to calculate $x(i)$. This is only apparent, and a consequence of requiring the control to use closer values in the recent past. In fact, this requirement nevertheless allows us to express $x(i)$ as a function of $x(i - 1)$ and $x(i - L)$, i.e., to have the well-defined causal dynamical law in discrete time [Eq. (14)]. The computational steps in the simplest case where $r = 0$ are as follows. Iterating Eq. (14) forward in time requires the initial conditions $x(0), x(-1), x(-2), \dots, x(1 - L)$. Only $x(0)$ and $x(1 - L)$ are needed to compute $x(1)$; next, $x(1)$ and $x(2 - L)$ are needed to compute $x(2)$; and so on. The same holds for both additive or parametric perturbations, as we will see below.

It is important to point out, however, that from this causal point of view, the applied perturbation at each time step may be small or large, since it is proportional to the state variable x itself. This may imply that the method is not well suited to deal with situations where our prior knowledge of the basic dynamical system to be controlled, $x(i) = F(x(i - 1))$, is incomplete. Experimental tests will ultimately confirm this point, and are beyond the scope of the present work. Our control method was devised with applications to dynamical memory devices in mind, both in continuous or discrete time; in these cases, the dynamical law is often known with great precision, such as in the case of the Ikeda laser equation [4] or hybrid systems such as acousto-optic devices [31]. This extended range of control is discussed from an analytical point of view for additive control in Sec. IV B, and parametric control in Sec. IV C.

B. Range of control for additive feedback

In order to compare Socolar, Sukow, and Gauthier's method with ours, we investigate the control of the fixed point of the logistic map with additive feedback control. Since their original work used parametric control, we need first to derive the stability criteria for their method with additive extended control. The dynamics for the controlled map $F(x)$ are

$$x(i) = F(x(i - 1)) + d(i - 1), \quad (16)$$

$$d(i) = K[x(i) - x(i - 1)] + rd(i - 1),$$

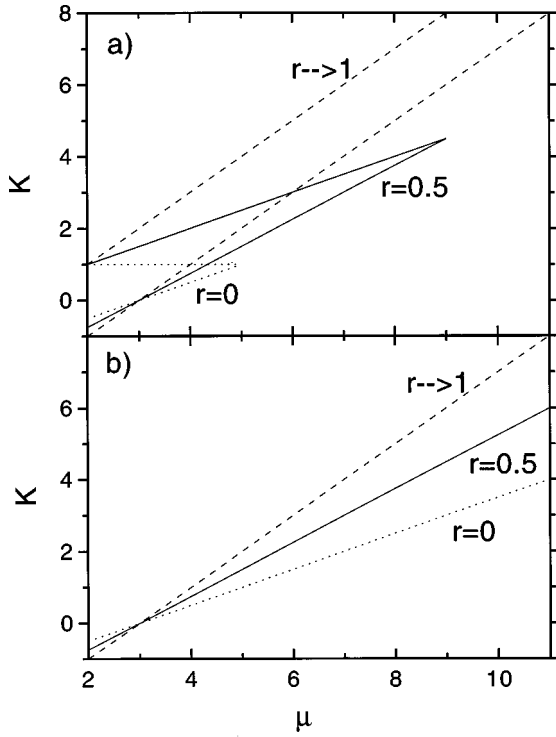


FIG. 8. Boundaries in the (K, μ) plane for stable control of the fixed point in the logistic map using additive perturbations. Dotted lines are for $r=0$, solid lines for $r=0.5$, and dashed lines for $r \rightarrow 1$. (a) The range of stable control is defined by the area between the lines using Eq. (16). (b) The range of stable control is defined by the area in the upper-half-planes using our method [Eq. (14)]. This range is much larger than in (a).

which can be rewritten as

$$x(i) = F(x(i-1)) + d(i-1), \quad (17)$$

$$d(i) = K[F(x(i-1)) - x(i-1)] + (K+r)d(i-1).$$

The controlled map has a fixed point at $(x^*, d^*) = ((\mu - 1)/\mu, 0)$ which is unstable for $\mu > 3$. By linearizing the controlled map around this fixed point, and letting $y(i) = x(i) - x^*$ and $e(i) = d(i) - d^*$, the above equations yield

$$\begin{pmatrix} y(i) \\ e(i) \end{pmatrix} = \begin{pmatrix} \nu & 1 \\ K(\nu-1) & K+r \end{pmatrix} \begin{pmatrix} y(i-1) \\ e(i-1) \end{pmatrix}, \quad (18)$$

where $\nu = F'(x^*) = 2 - \mu$. The stable control is obtained by first finding the eigenvalues of the matrix in Eq. (18), which are given by

$$\lambda_{\pm} = \frac{1}{2}[\nu + K + r \pm \sqrt{(\nu + K + r)^2 - 4(\nu r + K)}]. \quad (19)$$

The control is stable if $|\lambda_{\pm}| < 1$. This yields the domain of stability $\nu < 1$ (i.e., $\mu > 1$), $K > (1+r)(\mu-3)/2$, and $K < 1 + (\mu-2)r$ [see Fig. 8(a)].

Now we use instead our control term in Eq. (14), and apply the resulting control method to the fixed point of the logistic and the MG maps. The linearization around the fixed point (x^*, D^*) , with $y(i) = x(i) - x^*$ and $e(i) = D(i) - D^*$, yields

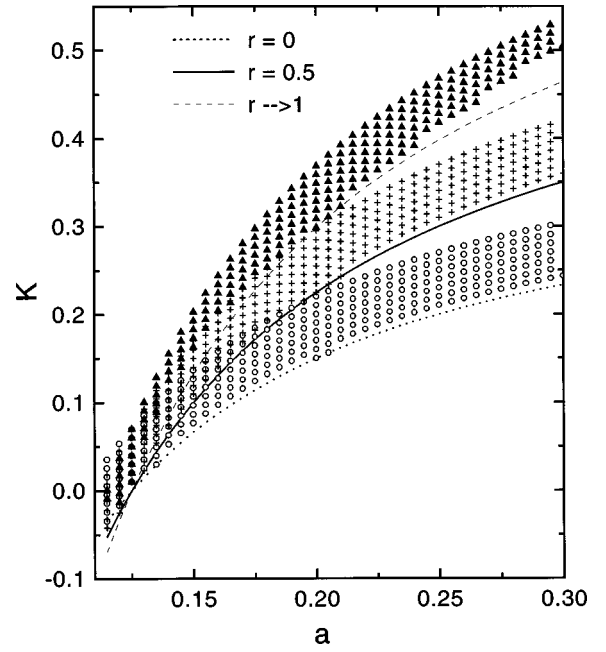


FIG. 9. Boundaries in the (K, a) plane for stable control of the fixed point of the MG map using Eq. (14) (additive control). The dotted, solid, and dashed curves are the stability boundaries for, respectively, $r=0$, $r=0.5$, and $r \rightarrow 1$; control occurs in the upper half-planes bounded by these curves. The open circles ($r=0$), pluses ($r=0.5$), and filled triangles ($r \rightarrow 1$) indicate regions of stable control of the fixed point of the DDE [Eq. (9), $\tau=300$] from which the MG map was obtained. For clarity, only the beginning of these stability regions have been plotted for each value of r ; in fact, they extend vertically into the upper-half plane, as for the map. There is good agreement between the region of stable control in the map and in the DDE at large delay.

$$\begin{pmatrix} y(i) \\ e(i) \end{pmatrix} = \frac{1}{b+K} \begin{pmatrix} \nu+K & r \\ K(b-\nu) & br \end{pmatrix} \begin{pmatrix} y(i-1) \\ e(i-1) \end{pmatrix}. \quad (20)$$

The eigenvalues that determine the stable control are given by

$$\lambda_{\pm} = \frac{1}{2(b+K)} [\nu + K + br \pm \sqrt{(\nu + K + br)^2 - 4r\nu(b+K)}]. \quad (21)$$

The stable control is bounded by the curves $K > -(1+r)(b+\nu)/2$ and $K > r\nu - b$ for $0 < \nu < b$, and by $K > -(1+r)(b+\nu)/2$ for $\nu < 0$. For the logistic map ($b=1$ and $\nu = 2 - \mu$), the range of stability of the controlled fixed point in the (K, μ) plane is much larger than in the previous case [see Fig. 8(b)].

For the MG map (Fig. 9), the boundaries for stable control of the fixed point are curved since they are plotted in the (K, a) space and $\nu = b(1/a - 9)$ ($b=0.1$). Figure 9 also plots the range of control for the MG-DDE, as determined by numerical simulation. It is seen that, for a given value of r , the boundary for the map and for the DDE are approximately the same at this level of resolution. Hence the stable control of the fixed point in the MG map can be used to predict the controllability of the fixed point in the DDE at large delays. We recall that this fixed point goes unstable at a Hopf bifurcation which occurs at $a=0.125$ for $\tau=300$.

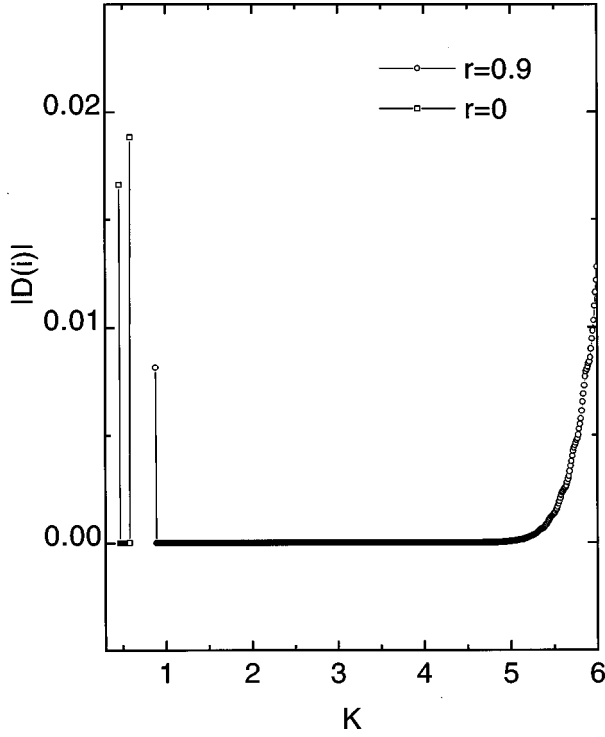


FIG. 10. Dispersion $|D(i)|$ vs K for the P_4 orbit of the logistic map $x(i) = \mu x(i-1)[1-x(i-1)]$, using Eq. (14) for $\mu = 3.95$, with $r=0$ and 0.9 . Note that, for $r=0$, the dispersion decreases to zero only for a narrow range of K values, and that the ranges of K where D is negligible do not overlap for the $r=0$ and 0.9 cases. The range of control with $r=0.9$ is much larger than with $r=0$, demonstrating the advantages of extended control [15] even for orbits with a higher bifurcation order.

The controllability of orbits with $N > 1$, for example the P_4 orbit of the logistic map, is also enhanced with our method. Without control, this orbit is unstable for $\mu > 3.54$. If we apply the method in Ref. [15], this orbit remains stable up to $\mu \approx 3.62$ for $r=0$. Using our method [Eq. (14) with $b=1$] without extended control ($r=0$), the control of this orbit can be maintained up to $\mu = 3.97$, and the allowable range of K is much larger (not shown). This range decreases with increasing L , so higher-period orbits are very difficult to control using both methods for $r=0$.

The performance of the method improves even more if $r > 0$ (see Fig. 10), allowing control of higher period UPO's and enhanced parameter ranges. For example, with $r=0.9$ the control of the P_4 orbit can be maintained up to $\mu = 4.5$, while the method in Ref. [15] controls up to $\mu = 3.75$ using $r=0.5$. Figures 10 and 12(b) show how the range of controllability of the P_4 orbit is enhanced with Eq. (14) for, respectively, the logistic map ($\mu = 3.95$, $r=0.9$) and the MG map ($a=0.145$, $r=0.8$).

C. Range of control for parametric feedback

We now consider the case of parametric feedback for our method, and compare it to the results for parametric control presented in Ref. [15]. Let $F(x(t-\tau)) = \mu f(x(t-\tau))$ (μ is the feedback parameter). Parametric control for the DDE can be written as

$$\begin{aligned} \dot{x}(t) &= -bx(t) + \{\mu + K[x(t-T) - x(t)] + rD(t-T)\} \\ &\quad \times f(x(t-\tau)), \\ D(t) &= K[x(t-T) - x(t)] + rD(t-T). \end{aligned} \quad (22)$$

By letting $b\tau \rightarrow \infty$ as in Sec. IV B, the CTDE with parametric control can be written as

$$\begin{aligned} x(t) &= [b + Kf((t-\tau))]^{-1} \{\mu + Kx(t-T) + rD(t-T)\} \\ &\quad \times f(x(t-\tau)) \\ D(t) &= K[x(t-T) - x(t)] + rD(t-T). \end{aligned} \quad (23)$$

The control of the fixed point in the corresponding map is

$$\begin{aligned} x(i) &= [b + Kf(x(i-1))]^{-1} \{\mu + Kx(i-1) + rD(i-1)\} \\ &\quad \times f(x(i-1)), \\ D(i) &= K[x(i-1) - x(i)] + rD(i-1). \end{aligned} \quad (24)$$

This can be rewritten as

$$x(i) = g(x(i-1))[\mu + Kx(i-1) + rD(i-1)], \quad (25)$$

$$\begin{aligned} D(i) &= Kx(i-1) - Kg(x(i-1))[\mu + Kx(i-1) + rD(i-1)] \\ &\quad + rD(i-1), \end{aligned}$$

where $g(x) = f(x)/[b + Kf(x)]$. We again focus on controlling the fixed point of the logistic map: $x_i = F(x_{i-1}) = \mu x_{i-1}(1-x_{i-1})$, $b=1$. The fixed points satisfy $x^* = F(x^*)$ and $D^* = 0$. The algebra can be simplified using the following relationships:

$$g(x^*) = x^*/[\mu + Kx^*], \quad (26)$$

$$g'(x^*) = \mu\nu/[\mu + Kx^*]^2,$$

where $\nu = F'(x^*)$. The linearization around the fixed point (x^*, D^*) with $y(i) = x(i) - x^*$ and $e(i) = D(i) - D^*$ yields

$$\begin{pmatrix} y(i) \\ e(i) \end{pmatrix} = \frac{1}{\mu + Kx^*} \begin{pmatrix} \mu\nu + Kx^* & rx^* \\ K\mu(1-\nu) & r\mu \end{pmatrix} \begin{pmatrix} y(i-1) \\ e(i-1) \end{pmatrix}. \quad (27)$$

The eigenvalues that determine the stable control are given by

$$\begin{aligned} \lambda_{\pm} &= \frac{1}{2(\mu + Kx^*)} [\mu(\nu + r) + Kx^* \\ &\quad \pm \sqrt{[\mu(\nu + r) + Kx^*]^2 - 4r\mu\nu(\mu + Kx^*)}]. \end{aligned} \quad (28)$$

The requirement that $|\lambda_{\pm}| < 1$ yields the stability curves for our parametric control method: $K > -\mu(1+r)(\nu+1)/(2x^*)$ and $K > \mu(r\nu-1)/x^*$ if $0 < \nu < 1$, and $K > -\mu(1+r)(\nu+1)/(2x^*)$ if $\nu < 0$. For the logistic map ($b=1$, $x^* = (\mu-1)/\mu$, $\nu = 2-\mu$), the stability boundary for the case of interest here ($\nu < 0$, i.e., $\mu > 2$) is thus $K > -\mu^2(1+r)(3-\mu)/(2(\mu-1))$. Stability occurs in the upper-half-plane bounded from below by this curve (Fig. 11). This curve is similar to the one with additive control

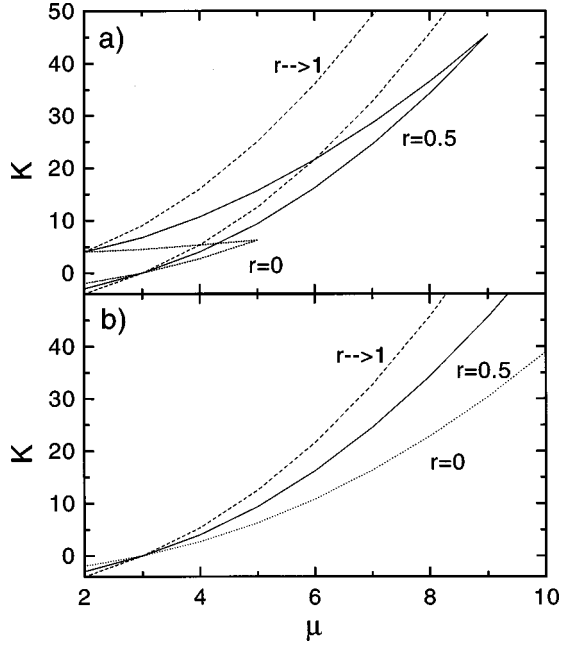


FIG. 11. Parametric control of the logistic map (Sec. IV C). Dotted lines are for $r=0$, solid lines for $r=0.5$, and dashed lines for $r \rightarrow 1$. (a) The range of stable control is defined by the area between the lines using Eq. (16). (b) The range of stable control is defined by the area in the upper-half-planes using Eq. (14). This range is much larger than in (a).

obtained from Eq. (21), except for the factor $\mu^2/(\mu-1)$. With the additive control, the curves for stable control are straight lines; for parametric control, that factor turns these lines into parabolas. The method again produces control over a larger parameter range than in Ref. [15], as Fig. 11 reveals. We note again that our method assumes a good knowledge of the map F .

D. Prediction of controllability of the DDE

This section shows that the absolute value of the feedback perturbation, $|D(i)|$ (also referred to as ‘‘dispersion’’ [14]), and the Lyapunov exponents of the map, are important for predicting the parameter range over which the DDE at large R and the map itself can be controlled. Numerical computation of the dispersion is straightforward. The Lyapunov exponent estimation must however be done carefully, e.g., using QR decomposition as we do below [32]. The Jacobian matrices may have singularities for higher period orbits because of finite numerical precision. We first convert the $2L$ -dimensional map [Eq. (14)] into $2L$ coupled one-dimensional maps,

$$\begin{aligned}
 y_0(i) &= (b+K)^{-1} \{F(y_0(i-1)) + Ky_1(i-1) + rz_1(i-1)\} \\
 z_0(i) &= (b+K)^{-1} \{-KF(y_0(i-1)) + bKy_1(i-1) \\
 &\quad + brz_1(i-1)\} \\
 y_j(i) &= y_{j+1}(i-1), \quad j=1,2,\dots,L-2, \\
 z_j(i) &= z_{j+1}(i-1), \quad j=1,2,\dots,L-2,
 \end{aligned} \tag{29}$$

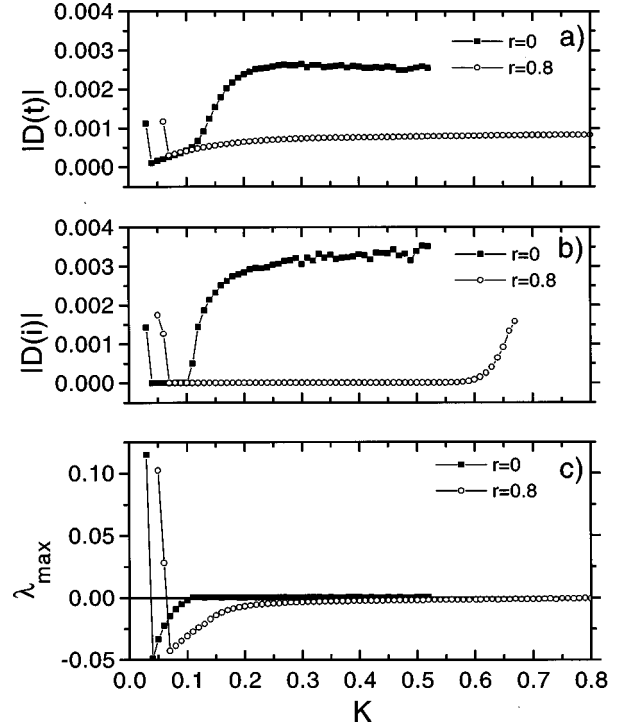


FIG. 12. Range of control for the P_4 orbit of the MG-DDE and the MG map for $a=0.145$ with $r=0$ and $r=0.8$. (a) Dispersion $|D(t)|$ vs K of the DDE using Eq. (9). (b) Dispersion $|D(i)|$ vs K of the map using Eq. (14). (c) Maximum Lyapunov exponent λ_{\max} vs K of the map using Eq. (29) and the QR decomposition method. Transients of 5000 periods have been discarded. In (a), the period of the UPO varies slightly with K according to $T = 1208.34 + 13.87 \exp[(0.07 - K)/0.1]$ obtained from fitted data. This variation was taken into account for the calculation of $D(i)$ vs K .

$$y_{L-1}(i) = y_0(i-1),$$

$$z_{L-1}(i) = z_0(i-1).$$

The QR algorithm is then applied using the Jacobian matrices of the $2L$ -dimensional map. Only a few decompositions are needed for Q to converge to the identity matrix [32]. The result is shown in Fig. 12(c), where λ_{\max} is in fact negative over a certain range of K values (negativity of all exponents is necessary to have control of the UPO). In the $r=0$ case, λ_{\max} converges quickly to zero as K increases. For $r=0.8$, λ_{\max} slowly increases to zero over the range of K presented here. This behavior is also seen in finite-dimensional dynamical systems [29]. Very good agreement is seen between the behaviors of λ_{\max} and the dispersion $|D(i)|$ of the map [Fig. 12(b)] for both values of r plotted, since the dispersion is small when λ_{\max} is negative. This is also true when comparing the behavior of these quantities to that of the dispersion $|D(t)|$ for the DDE [Fig. 12(a)]. While the dispersion $|D(i)|$ is zero when control is achieved, the dispersion $|D(t)|$ for the DDE can only approach zero, due to the differentiability of the solution and the finite precision in the integration procedure. Further, $|D(t)|$ increases more rapidly from its minimum than $|D(i)|$ for both $r=0$ and 0.8 . Nevertheless, it is clear that both $|D(t)|$ and $|D(i)|$ have quali-

tatively similar behaviors as a function of the control gain K . Hence, the $2L$ -dimensional singular limit map again provides good insight into the control of the UPO's of the DDE.

V. APPLICATION OF CONTROL METHOD TO NEURAL NETWORKS

The control method discussed in Sec. IV is now applied to a small chaotic neural network evolving in discrete time [16,17]. The dynamics of the n th neuron in a network of M chaotic neurons is given by

$$y_n(i) = \sum_{m=1}^M W_{nm} \sum_{q=0}^{i-1} k^q h_m(x_m(i-1-q)) + \sum_{m=1}^N V_{nm} \sum_{q=0}^{i-1} k^q I_m(i-1-q) - \alpha \sum_{q=0}^{i-1} k^q g_n[x_n(i-1-q)] - \theta_n, \quad (30)$$

$$x_n(i) = f_n(y_n(i)), \quad (31)$$

where $x_n(i)$ is the output of the n th neuron at time i , $y_n(i)$ is the internal state of the n th neuron at time i , and θ is the threshold for firing. Also, M represents the number of neurons in the network, while N is the number of externally applied inputs I to a neuron. Functions h and g characterize, respectively, the propagation of action potentials down axons and the refractoriness of the neuron (the latter characterizes the inability of the neuron to fire spikes in close temporal

succession). W_{nm} describes the feedback connection strength between neurons in the network, and V_{nm} that between external inputs and neurons. Finally, α and k are constants. In the original model [16], the output function $f(y)$ was a unit step function; instead, we have used as in Ref. [17] a sigmoidal function with adjustable steepness: $f(y_n(i)) = 1/(1 + e^{-y_n(i)/0.02})$. Thus the output of a given neuron is an analog value between 0 and 1.

The above network dynamics depend on the whole previous history of the system, through the decaying effects of inputs and neuron refractoriness. It was shown in Ref. [16] that the neuron states at time i governed by these dynamics can be rewritten solely in terms of the immediately preceding states of all the neurons in the network at time $i-1$ as follows:

$$y_n(i) = ky_n(i-1) + \sum_{m=1}^M W_{nm} h_m(f_m(y_m(i-1))) + \sum_{m=1}^N V_{nm} I_m(i-1) - \alpha g_n(f_n(y_n(i-1))) - (1-k)\theta_n, \quad (32)$$

and $x_n(i) = f_n(y_n(i))$ as above. As in Ref. [17], we choose $h(x) = x$ and $g(x) = x$, $M = 3$, $\alpha = 1.0$, $\theta = 0.0$, and $W_{12} = W_{23} = W_{31} = 0.5$, and the other W_{nm} 's and all V_{nm} 's are set to zero. The initial functions are $y_1(0) = 1.0$, $y_2(0) = 0.0$, $y_3(0) = 0.0$. Further, we apply the control to the first chaotic neuron in the network. The dynamics are then

$$\begin{aligned} y_1(i) &= (1+K)^{-1} [ky_1(i-1) - f(y_1(i-1)) + 0.5f(y_2(i-1)) \\ &\quad + Ky_1(i-L) + rD(i-L)], \\ D(i) &= K[y_1(i-L) - y_1(i)] + rD(i-L), \\ x_1(i) &= f(y_1(i)), \\ y_2(i) &= ky_2(i-1) - f(y_2(i-1)) + 0.5f(y_3(i-1)), \\ x_2(i) &= f(y_2(i)), \\ y_3(i) &= ky_3(i-1) - f(y_3(i-1)) + 0.5f(y_1(i-1)), \\ x_3(i) &= f(y_3(i)), \end{aligned} \quad (33)$$

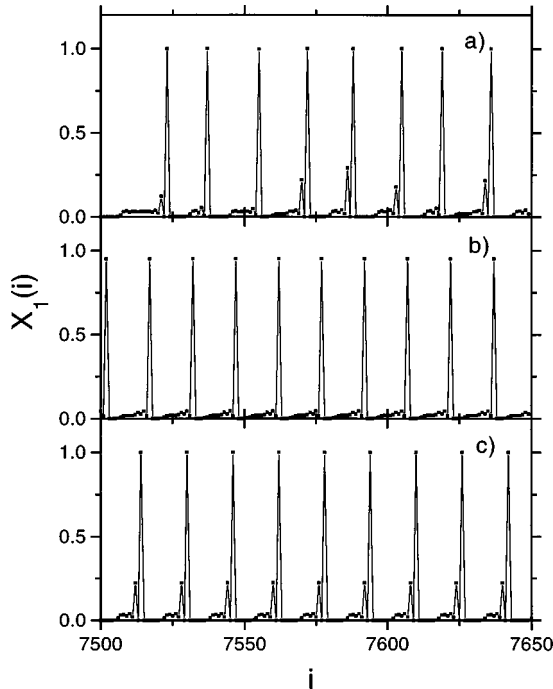


FIG. 13. Controlling chaos in a Nagumo-Sato network composed of three neurons. $X_1(i)$ is the output of the first chaotic neuron, which takes values between 0 and 1. (a) The chaotic solution of the first neuron $X_1(i)$ vs i for $K=0$ and $r=0$. (b) Controlled solution using Eq. (14) with $L=15$, $K=0.38$, and $r=0.5$. (c) Same as in (b), but for $L=16$, $K=0.2$, and $r=0.5$.

The bifurcation parameter k in Refs. [16,17], distinct from the additive feedback control gain K , sets the decay rate of refractoriness and memory effects from past inputs. Without the control of UPO's using additional delayed feedback, $k = 0.769\ 231$ produces chaotic behavior with Lyapunov spectrum $(0.13, -0.23, -1.29)$ [17]. The behavior of one neuron in the network is shown in Fig. 13(a), where neuron output is plotted as a function of discrete time. The sharp spikes correspond to neuron firings. If our control method is applied to the first neuron in Eq. (33), the network behaves periodically, as shown in Figs. 13(b) and 13(c) for $L=15$ and 16 , respectively.

Our method is thus applicable to biophysically detailed models of activity in networks of neurons. This suggests in

turn that the control method can be applied to real networks of excitable cells by monitoring either the firing state x or the internal voltage state y , provided one has sufficient knowledge about the functions and parameters in the above equations which describe its uncontrolled behavior. Combining the results of this section with those in Sec. III, we anticipate that the same control method can be used for both discrete-time networks, such as the one studied here, and versions of these networks with added differential terms.

VI. CONCLUSION

We have first presented results on multistability and hysteresis of stable solutions of the Mackey-Glass delay-differential equation, as well as on the controllability of its unstable periodic orbits. We have focused on the large delay-to-response time ratio regime ($R=30$). In particular, the number of multistable solutions, either periodic or chaotic harmonics of a fundamental wave form, is found to be finite, as is the number n_{\max} of stable harmonics accessible to the system as a is varied and other parameters are kept fixed.

We have then shown that the ‘‘extended control’’ of UPO’s devised for maps [15] and ordinary differential equations [29,30] allows finely structured orbits of the DDE to be controlled. The maximum bifurcation order of controlled UPO’s in the DDE with $\tau=300$ is three (third period-doubling bifurcation), corresponding to a P_8 -type solution in which the plateaus cycle between eight values. We have further shown that the difference equations (in both continuous or discrete time), obtained in the singular perturbation limit of the DDE, are useful to predict the range of control of the DDE at large R . More work is needed to design a control that can stabilize UPO’s with higher bifurcation orders. Nevertheless, the results presented here will be useful for the design of high capacity versatile memory devices based on the multistability inherent to delayed dynamical systems or continuous-time difference equations, as well as to discrete-time dynamical systems.

The information storage capacity of DDE’s at large R , without control [9] or with additional or extended delayed feedback control, is limited by the requirement that only one pattern be stored at a time. The possibility of using more than one of the coexisting solutions at a time will be explored in future work.

The controlled dynamics in the singular limit $R \rightarrow \infty$ further suggest an improved method of controlling discrete-time systems. This method extends the parameter range over

which control occurs as compared to standard methods, and allows for the control of UPO’s with higher bifurcation orders. Its power relates to the fact that the control perturbations, extended or not, are calculated based on more recent information about the state of the system. The method works for both additive or parametric control. More work is required to determine the performance of the method in the face of, e.g., uncertainty about the uncontrolled dynamics, or, relatedly, noise. This is of importance in the context of the control of, e.g., real excitable systems.

Such future work could benefit greatly from results in the control systems theory literature, which has confronted problems of delayed feedback control for a long time (see, e.g., Ref. [33]). Indeed, many DDE solutions with plateaus, as well as orbits of CTDE’s and maps, have several features in common with so-called ‘‘discrete signals,’’ i.e., signals which vary only at discrete times. Thus the combination of these solutions and the continuous feedback needed to obtain them make the dynamical systems of study here similar to sampled-data systems [34]. Consequently, concepts from the literature on the digital control of dynamical systems, such as the z transform and the controllability matrix, are relevant to analyze the stability of the delay and extended delay systems studied here, both for the large delay case and the discrete-time singular map case. That literature generally focuses on canonical dynamical forms involving constant coefficient matrices and the control of fixed points, while the problems of interest in our study involve the control of nonlinear flows onto various kinds of periodic trajectories. Thus the methods from that literature will be particularly helpful for fixed point control issues, and can also guide the analysis for the linearization around periodic orbits and the stabilization of UPO’s.

Our discrete-time control method meets the primary ‘‘applied’’ objectives of our work, namely, to allow for the control of finely structured orbits in difference equations and maps used to model, e.g., neural networks [16,17,23] and dynamical memory devices [9,13]. The method was illustrated here on a chaotic neural network, given the interest in controlling or producing aperiodic dynamics in real systems of, e.g., nerve or cardiac cells, or in simply understanding and controlling their multistability.

ACKNOWLEDGMENTS

This work was supported by the NSERC, Canada, as well as by CIDA (B.M.)

-
- [1] K. Ikeda and K. Matsumoto, *Physica D* **29**, 223 (1987).
 - [2] K. Ikeda, H. Daido, and O. Akimoto, *Phys. Rev. Lett.* **45**, 709 (1980).
 - [3] M. C. Mackey and L. Glass, *Science* **197**, 287 (1977).
 - [4] K. Ikeda, K. Kondo, and O. Akimoto, *Phys. Rev. Lett.* **49**, 1467 (1982).
 - [5] C. Lourenço and A. Babloyantz, *Neural Comput.* **6**, 1141 (1994).
 - [6] S. A. Campbell, J. Bélair, T. Ohira, and J. G. Milton, *J. Dyn. Diff. Eq.* **7**, 213 (1995).
 - [7] C. M. Marcus and R. M. Westerwelt, *Phys. Rev. A* **39**, 347 (1989).
 - [8] H. M. Gibbs, F. A. Hopf, D. L. Kaplan, and R. L. Shoemaker, *Phys. Rev. Lett.* **46**, 474 (1981).
 - [9] T. Aida and P. Davis, *IEEE J. Quantum Electron.* **28**, 686 (1992).
 - [10] J. Foss, A. Longtin, B. Mensour, and J. Milton, *Phys. Rev. Lett.* **76**, 708 (1996).
 - [11] J. Losson, M. C. Mackey, and A. Longtin, *Chaos* **3**, 167 (1993).

- [12] J. Foss, J. M. Milton, and F. Moss, *Phys. Rev. E* **55**, 4536 (1997).
- [13] B. Mensour and A. Longtin, *Phys. Lett. A* **205**, 18 (1995).
- [14] K. Pyragas, *Phys. Lett. A* **170**, 421 (1992).
- [15] J. E. S. Socolar, D. W. Sukow, and D. J. Gauthier, *Phys. Rev. E* **50**, 3245 (1994).
- [16] J. Nagumo and S. Sato, *Kybernetik* **10**, 155 (1972).
- [17] K. Aihara, T. Takabe, and M. Toyota, *Phys. Lett. A* **144**, 333 (1990).
- [18] K. Konishi, M. Ishii, and H. Kokame, *Phys. Rev. E* **54**, 3455 (1996).
- [19] A. F. Ivanov and A. N. Sharkovskii, in *Dynamics Reported*, edited by H. O. Walther and U. Kirchgraber (Springer-Verlag, Berlin, 1991), Vol. 3, pp. 165–220.
- [20] M. LeBerre, E. Ressayre, A. Tallet, and H. M. Gibbs, *Phys. Rev. Lett.* **56**, 274 (1986).
- [21] See, e.g., *From Oscillations to Excitability—A Case Study in Spatially Extended Systems*, edited by S. C. Müller, P. Couillet, and D. Walgraef, focus issue of *Chaos* **4**, 439–568 (1994).
- [22] A. Garfinkel, M. Spano, W. L. Ditto, and J. N. Weiss, *Science* **257**, 1230 (1992); S. J. Schiff, K. Jerger, D. H. Duong, T. Chang, M. L. Spano, and W. Ditto, *Nature (London)* **370**, 615 (1994).
- [23] R. V. Solé and L. Menéndez de la Prida, *Phys. Lett. A* **199**, 65 (1995).
- [24] L. Glass and C. P. Malta, *J. Theor. Biol.* **145**, 217 (1990).
- [25] W. Gerstner, *Phys. Rev. Lett.* **76**, 1755 (1996).
- [26] J. Bélair and S. A. Campbell, *SIAM (Soc. Ind. Appl. Math.) J. Appl. Math.* **54**, 1402 (1994).
- [27] P. Nardone, P. Mandel, and R. Kapral, *Phys. Rev. A* **33**, 2465 (1986).
- [28] B. Mensour and A. Longtin, *Physica D* **113**, 1 (1998).
- [29] K. Pyragas, *Phys. Lett. A* **206**, 323 (1995).
- [30] M. E. Bleich and J. E. S. Socolar, *Phys. Lett. A* **210**, 87 (1996).
- [31] R. Vallée and C. Delisle, *Phys. Rev. A* **31**, 2390 (1985).
- [32] J. P. Eckmann and D. Ruelle, *Rev. Mod. Phys.* **57**, 617 (1985); H. D. I. Abarbanel, R. Brown, and M. B. Kennel, *J. Nonlinear Sci.* **2**, 343 (1992).
- [33] M. N. Oguztöreli, *Time-Lag Control Systems* (Academic, New York, 1966).
- [34] G. F. Franklin and J. D. Powell, *Digital Control of Dynamic Systems* (Addison-Wesley, Reading, MA, 1980).